13

EXPLORING PHYSIOLOGICAL FEATURES FROM ON-BODY RADIO CHANNELS

MAX O. MUNOZ AND YANG HAO

School of Electronic Engineering and Computer Science, Queen Mary University of London, London, UK

13.1 INTRODUCTION

The integration and connectivity of different electronic devices—such as smart phones, wrist-worn watches, and even home entertainment systems—have become a part of our daily life. The current devices offer not only human interaction, but also inter-operability between them, creating dedicated and independent wireless networks (wireless personal area networks (WPANs) and wireless body area networks (WBANs) [1, 2]). The new smart devices are capable of processing and controlling unique applications which are transmitted through seamless wireless channels operating at exclusive radio frequencies.

The continuous development of conformal and compact low-power electronics have enabled the miniaturization of hardware systems and, thus, led to a new generation of wearable sensors (Figure 13.1) [3, 4]. Some of these body-worn sensors are equipped with a type of piezoelectric transducer for harvesting energy from biomechanical and physiological processes—such as kinetic movements, external forces, vibrations, and thermal energy—into a source of power [4–6].

Most of the research efforts have been directed toward continuous monitoring and quantification of physiological body signals, as well as the development of personalized healthcare devices [7–9]. In recent years, the demand for non-invasive sensing

Electromagnetics of Body-Area Networks: Antennas, Propagation, and RF Systems, First Edition.
Edited by Douglas H. Werner and Zhi Hao Jiang.

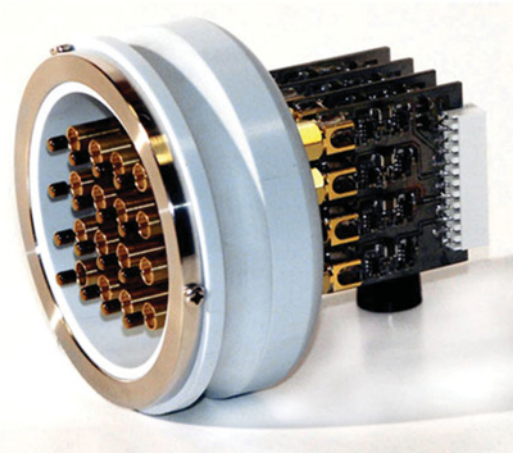

FIGURE 13.1 A look inside the housing of a prototype of the electric potential integrated circuit (EPIC) electrocardiogram tracking device shows that it is actually an array of 16 sensors that together ensure accuracy and reliability. *Source:* Jones 2011 [3] and Gyselinckx et al. 2005 [4]. Reproduced with permission of IEEE.

solutions that can effectively replace existing physiological sensors have attracted great interest, not only from the academic research, but also from the industry. Continuous non-invasive remote sensing systems have remained an elusive technology; however, the development of novel and pioneering RF front-end architectures combined with advanced digital signal processing algorithms have demonstrated several potential benefits of non-contact sensing. These new contact-less sensing systems are able to detect and continuously monitor biological and biomechanical signals such as heartbeat variability, respiration rate, blood pressure, perspiration, and temperature [10].

Non-invasive monitoring systems that detect heart and respiration activity are particularly important in evaluating patient's pathologies, especially if the patient has conditions that can be perturbed or worsened by contact sensors, for example, neonates (infants at risk of sudden infant death syndrome) and burn victims [11–13]. Moreover, non-invasive sensing has also been evaluated in the search of survivors from different natural disasters (earthquakes, tsunamis) [14]. It is evident that this new trend, and the use of on-body wireless sensors within hospitals and home environments, can significantly reduce healthcare costs and also improve patient's daily lifestyle.

The chapter describes different non-invasive RF technologies that have evolved and shown the potential for remote monitoring of vital signs. Section 13.2 gives a brief overview of important physiological signals, with an emphasis on respiration rate and heartbeat. Section 13.3 presents distinct non-invasive sensing techniques and highlights some of the leading applications which can be adopted not only in clinical

environments but also in home healthcare applications. Finally, concluding remarks of the chapter are presented in Section 13.4.

13.2 PHYSIOLOGICAL INFORMATION PARAMETERS

Extensive studies of the cardio-respiratory performance can be found in physiological literature which dwell in detail on the relationship between human activity and vital processes implicated in human cardiovascular and respiratory systems. Generally, the number of breaths and heartbeats per minute varies with the subject's age, gender, body mass index (BMI) (i.e., the ratio of body's weight and the square of height) and, of course, the subject's activity level. The pulse rate of a resting adult has an average frequency of 1–1.5 Hz, or 60–90 beats per minute (BPM). On the other hand, the resting respiration rate is about 6–12 breaths/min [15,16]. The biomechanical process of the cardiovascular and the respiration cycles produce abdominal displacements of 0.2–0.5 mm and 4–12 mm, respectively. During a normal walk, the normal pulse increases up to 95 BPM and the respiration rate varies between 12–18 breaths/min. The practice of any sport or fitness activities, such as jogging or swimming, causes the heartbeat rate to increase to almost twice that of a resting adult: 120–190 BPM (2–3.1 Hz, respectively) [16].

The cardiac recordings for a male test subject of 168 cm height and 80 kg weight is shown in Figure 13.2. The graphs depict time and spectral domain plots for two different scenarios: resting while standing and jogging at a constant speed of 5 km/h. The heart rate variability for both scenarios is listed in Table 13.1 considering a 5 minute time frame.

In the case of a resting scenario, the plot shows a main harmonic at 1.46 Hz describing a heart rate of 87.6 BPM. In contrast, a jogging scenario depicts two main frequency components: the first at 1.04 Hz and the second at 1.71 Hz. The former is mainly attributed to electrode movement due to constant human motion and the latter harmonic represents the cardiac signal, which outlines a heart rate of 102.6 BPM.

The transformation from time to frequency domain has introduced a heart rate (HR) deviation of 1.77% and 3.4% for resting and jogging scenarios, respectively. This deviation is mainly attributed to FFT coefficient rounding errors and floating point arithmetic quantization errors. It is evident that the ECG mainly records electrical variation of the heart over a period of time across the electrodes, whereas non-invasive EM-based physiological sensing systems detect the mechanical movement of the chest cavity [17,18].

13.3 METHODS FOR NON-INVASIVE PHYSIOLOGICAL DETECTION

In recent years, great attention has been given to the development and evaluation of non-invasive electromagnetic (EM) sensing systems. Nowadays, everyone is exposed to a complex mix of wireless communication sources such as Wi-Fi, GSM, GPS,

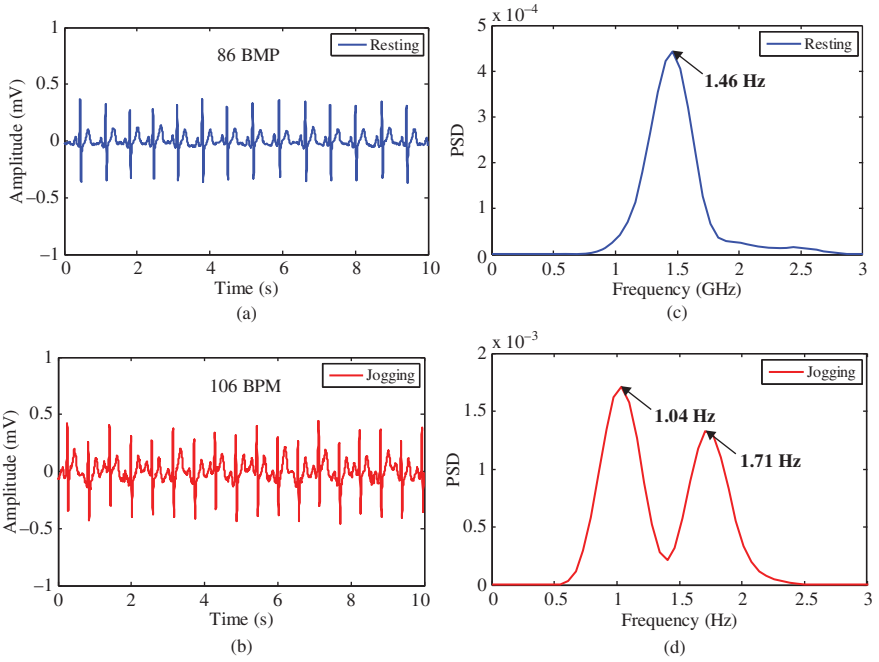

FIGURE 13.2 Heartbeat signal of the test subject while: (a) standing on the treadmill machine (resting stage), the average heartbeat was 86 BPM; (b) jogging at a constant speed of 5 km/h, the heartbeat rate was 106 BPM. Power spectral density (PSD) response using Welch's method for recorded ECG signals while the test subject is (c) standing on the treadmill machine (resting stage); (d) jogging at a constant speed of 5 km/h.

Bluetooth, and ZigBee which continuously radiate and propagate EM signals across our surrounding environment. In theory, the radio propagation information from each source can be used as a potential contact-less sensing method.

Several RF-based techniques have been proposed and tested at different microwave frequencies. The basic principle of this technology relies on the transmission of electromagnetic waves toward the sensing target. The reflected amplitude and phase are measured and recorded by other on/off-body receiving antenna architectures. The collected data embeds information not only from the radio channel link, but from the subject's bio-electromagnetic signature as well.

TABLE 13.1 Heart rate variability for resting and jogging scenarios calculated from a 5 min segment frame.

Scenario	HR mean	HR SD (σ)
Resting	86.07	4.83
Jogging at 5 km/h	106.3	4.29

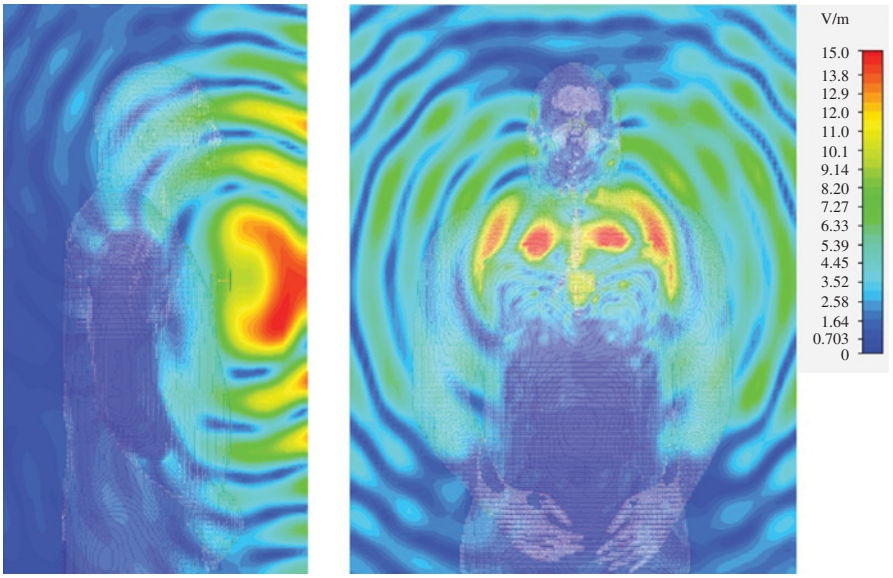

(a) (b)

FIGURE 13.3 Simulation results of the EM wave propagation alongside the trunk section of the Hugo model implemented in CST Microwave Studio. The radiating element is a microstrip patch antenna. (a) Antenna on-body; (b) antenna off-body. For a color version of this figure, see the color plate section.

It is evident that the electromagnetic wave propagation of on/off-body antennas are highly influenced by the behavior of the transmission path. For instance, the antenna of an on-body wireless node placed at chest level (Figure 13.3a) radiates electromagnetic waves that travel in free space and alongside the body surface. In the case of an off-body antenna (Figure 13.3b), the travelling EM wave impinges on the surface of the body producing surface, scattered, and reflected waves (i.e., multipath, shadowing).

Most of the non-invasive EM sensing systems have been implemented within research laboratory environments adopting one of the following methods: received signal strength (RSS), continuous-wave (CW), and wide band pulsed (UWB) signals. In order to extract and classify physiological features, acquired data are post-processed using a wide range of advanced digital signal processing algorithms.

13.3.1 Received Signal Strength-Based Methods

The radio channel characteristics of different on/off-body wireless communication devices can be described using the RSS values (packet-based transmissions). The signal strength is dependent on a number of factors which include the output power of the transmitter, the sensitivity of the receiver, the gain of the antennas, and the attenuation of the signal as it travels through the air from the transmitter to the receiver (path loss). Wireless devices operating in close proximity to the human body considerably

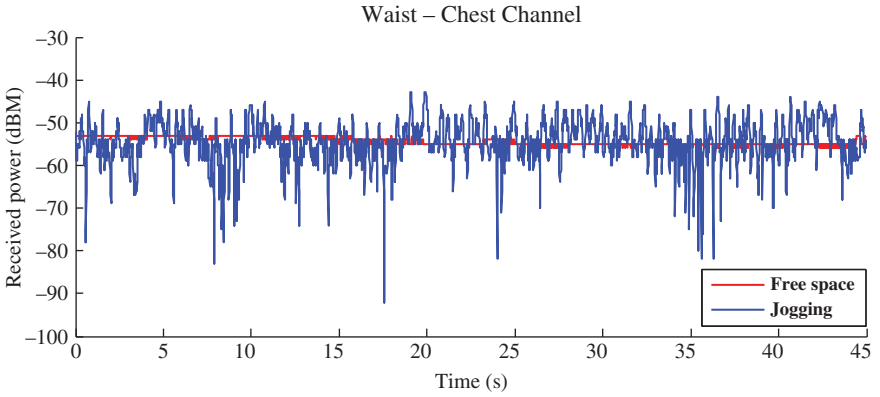

FIGURE 13.4 Recorded received signal strength (RSS) for a waist-to-chest channel recorded by custom-built wireless sensor nodes when the test subject is jogging and motionless in Queen Mary's Human Performance Laboratory.

attenuate the electromagnetic wave transmission due to inhomogeneous lossy tissue medium, and hence, drastically affect the received power signal. Moreover, external perturbations, such as human mobility and operation in cluttered environments, produce variant and complex EM wave propagation [19].

Empirical results of waist-to-chest radio channels have shown that dynamic scenarios create variations of ±15 dB from the average received signal; which is significantly greater than received signals of motionless users in free-space environments, where variations are ±3 dB (Figure 13.4) [18]. The practice of any sport activity produces a high level of fluctuations on the received signal, which are the consequence of the continuous movement of the human body.

Munoz et al. demonstrate the impact of motion on the radio propagation characteristics at 2.45 GHz from three different sport activities, namely, jogging, cycling, and rowing [17,18]. The packet-based RSS values are recorded for four on-body channels using custom-built wireless sensor nodes that are connected to a 2.15 dBi microstrip patch antenna (Figure 13.5b). The average power loss from on-body channels during dynamic tests have high variation amongst different links; however, back locations present the most correlated data between different actions (box plots, Figure 13.5c). The observed correlation is a consequence of the reduced movement on the back, in contrast to wrist and ankle sensor locations. In the case of the waist–ankle channel, data is highly correlated for two scenarios: jogging and cycling. This behavior is expected as a consequence of the constant speed of the user (5 km/h). The results suggest that the combination of unique radio propagation characteristics from two or three channels and implementing machine learning techniques is sufficient to determine the respective activity and even to classify the types of limb movements. The latter is accomplished using classification procedures such as support vector machine (SVM) and K-nearest neighbor methods, which are useful for rehabilitation procedures of individuals with functional limitations (kinesiotherapy applications) [20,21].

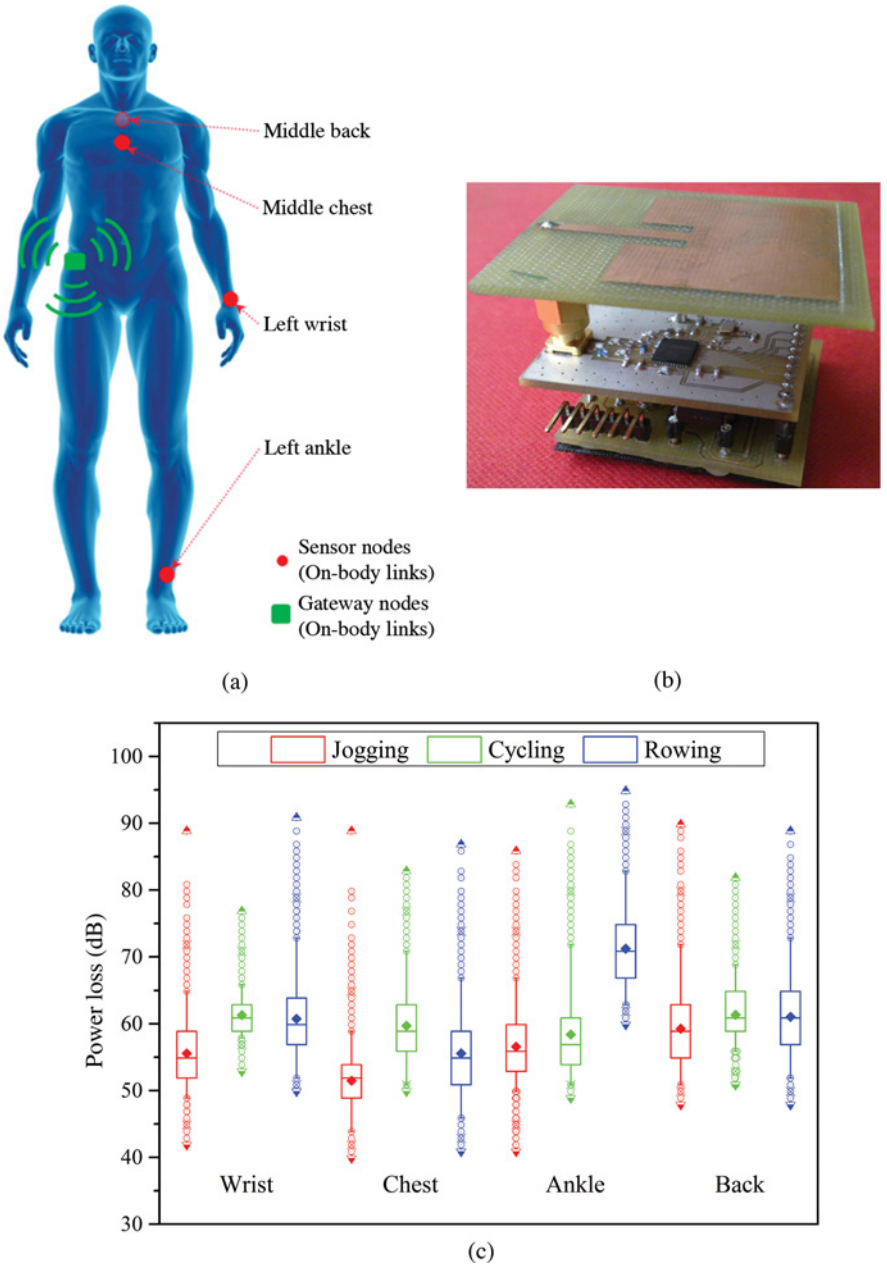

FIGURE 13.5 (a) Location of custom-built wireless sensors nodes used for dynamic WBAN radio channel characterization for each athletic activity; (b) custom-built wireless sensor nodes; (c) power loss for different on-body radio channels estimated from recorded RSS while test subject is under physical workout. The spacing between the different parts of the box indicates the degree of dispersion and skewness of the data.

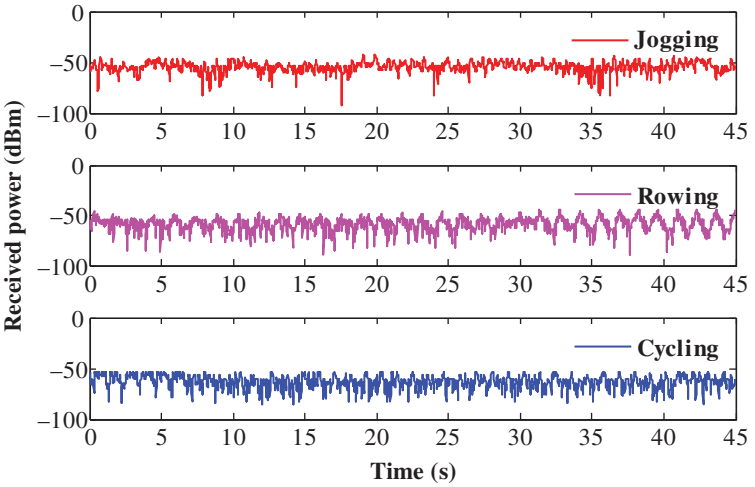

FIGURE 13.6 Received signal strength (RSS) for waist–chest channels recorded with custom-built wireless sensor nodes from three different activities: (a) jogging, (b) rowing, and (c) cycling. The measurements were performed in Queen Mary's Human Performance Laboratory.

Furthermore, Munoz et al. show that breathing rate can also be extracted from RSS measurements of waist-to-chest channels, even when the person is doing some exercises, but not the heart rate. The received signal of waist-to-chest channels for rowing, cycling, and jogging, with mean values of −50.19 dBm, −62.68 dBm, and −58.57 dBm, respectively, (Figure 13.6) is normalized and filtered using a 10th-order elliptic band-pass infinite impulse response (IIR) filter. In order to avoid frequency component confusion, two different band-pass filters are implemented: the first filter with cut-off frequencies of 0.1 Hz (lower frequency) and 0.8 Hz (higher frequency) for breathing analysis, and the second filter with cut-off frequencies of 0.8 Hz (lower frequency) and 3 Hz (higher frequency) for heart-beat movement.

The frequency domain analysis is based on the estimation of the power spectrum density (PSD) from filtered data. The PSD evaluation methods can be divided into parametric, for example, Autoregressive (AR) model, and non-parametric methods. The non-parametric methods, for example, Welch's periodogram, are in general, faster to compute and in the case of Welch's FFT method, it reduces the variance of the spectral density by averaging out uncorrelated noise.

This method divides the time series samples into overlapping sub-sequences. Each sub-sequence is windowed and then the estimated spectral density is averaged using a Hanning window (13.1) which smooths uncorrelated data located at the edges, diminishing aliasing of different rooted information and minimizing the amplitude dispersion into other harmonics (reduced spectral leakage). Additionally, the window function limits the extent of the sequence providing a more stationary spectral characteristic. The terms n and N in (13.1) represent the discrete-time index and the

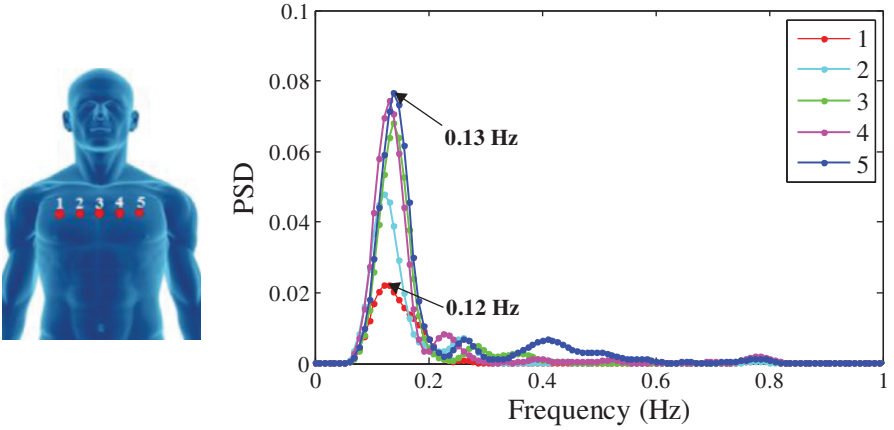

FIGURE 13.7 Power spectral response recorded by Wireless Sensor Networks (WSNs) for five different positions alongside the trunk section while the test subject is resting (standing on the treadmill machine).

length of the window, respectively. The window length was selected such that reasonable spectral performance is achieved. In the data analysis, N is limited to 4096 samples (without zero padding) with window sections of 1024 and window overlaps of 512.

$$w_n = 0.5\left[1 - \cos\left(2\pi\frac{n}{N}\right)\right] \quad \text{for } 0 \le n \le N \tag{13.1}$$

The spectral content of a resting scenario (test subject standing on the treadmill machine) is taken for five different locations, mainly along the upper chest section. The resulting plot (Figure 13.7) depicts the main component at these locations, which occurs between 0.12 Hz and 0.13 Hz; this would be equivalent to a breathing rate of 7.2–7.8 breaths/min.

In the case of dynamic scenarios, the spectral response of a jogging subject (Figure 13.8a) shows a sub-harmonic at 0.14 Hz (lower frequencies), which could be regarded as the thoracic displacement produced by the breathing process (approximately 8.5 breaths/min). The frequency domain plot of a rowing activity has two main components at lower frequencies (namely, 0.17 Hz and 0.71 Hz) (Figure 13.8b). The lower component, 0.17 Hz, is mainly attributed to the thoracic movement produced either by the human motion or the breathing process, which would relate to an average respiration rate of 10.2 breaths/min. The last spectrum plot corresponds to a cycling scenario (Figure 13.8c), where main components are observed at 0.16 Hz. The motion observed during cycling is mainly dominated by the leg movement, whereas the chest area remains fairly motionless, in contrast to the other activities. This type of body posture creates a cavity section for the electromagnetic propagation which maximizes the number of waves travelling along the body and hence the 0.16 Hz

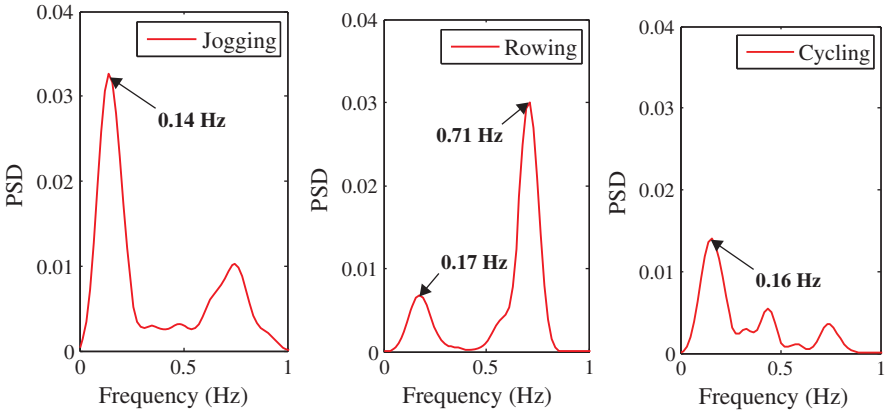

FIGURE 13.8 Power spectral density response using Welch's method for RSS signals while the test subject is (a) jogging; (b) rowing, and (c) cycling. All the activities are performed at a constant speed of 5 km/h.

harmonic is interpreted as a result of the respiration process which would be equivalent to 9.6 breaths/min.

It is shown that a wireless network topology has a better sensing performance than a single link. This non-invasive approach is applied by an application called BreathTaking which uses RSS values from a wireless sensor network of 20 MEMSIC TelosB following the IEEE 802.15.4 protocol [22] (Figure 13.9a).

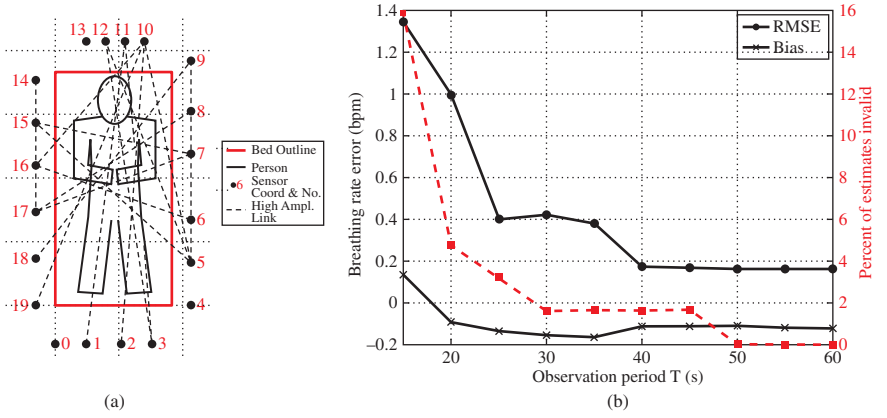

FIGURE 13.9 (a) Experimental layout showing sensors, bed, and person's approximate position; (b) RMSE and bias of valid BreathTaking frequency estimates for controlled breathing/patch antenna experiment (actual breathing rate of 15 breaths/min), and percent of rate estimates that are invalid (right y-axis), versus observation period T. *Source:* Patwari et al. 2014 [22]. Reproduced with permission of IEEE.

The application uses two different types of antennas: a directional patch antenna with an 8 dBi gain and an omnidirectional horizontal pattern dipole antenna with a 2.25 dBi gain. Although it remains possible to detect breathing using dipole antennas, it is clearly better, in terms of robustness to motion occurring outside of the test environment, to use directional antennas.

The non-invasive monitoring system reliably detects breathing and estimates breathing rate to within 0.3 breaths/min based on 30 seconds of data (Figure 13.9b). Moreover, the RSS-based sensing model is not only used to estimate respiration rate, but also to locate the breathing pattern of a person in home environments [23]. The extraction of the physiological parameter is based on a normalized sum of the squared amplitudes $|\widehat{A}|^2$ (maximum likelihood estimator (MLE)) over all measured radio links, which includes frequency, link amplitudes, and link phases. The method also removes motion interference produced by other movements, which generally cause large variations in RSS values, apart from a person's breathing. It is interesting to note that phase estimates of each link are affected by the breathing movement producing a bimodal distribution; in each case they are separated by 180°.

A further study is presented by Kaltiokallio et al. [24, 25] who employ RSS measurements from a single pair of off-the-shelf wireless sensors which are based on Texas Instruments' CC2431. The stack protocol of each transceiver follows the IEEE 802.15.4 standard [26] for an operation at 2.4 GHz ISM band. The non-invasive wireless sensors use high performance directional flat patch antennas (8 dBi gain and 75° horizontal beam width).

The wireless sensors are put on opposite sides of a bed at a height of 0.85 m and 1.95 m apart from each other (Figure 13.10). The transmitter node transmits RSS packets over each of the 16 frequency channels with a sampling rate of 16 ms per channel. A high resolution RSS reference signal is also acquired by a real-time spectrum analyzer (RSA) that is connected to the receiver node through a directional coupler.

Motion interference is mitigated by using a hidden Markov model (HMM) to detect the time instances when breathing estimation is not possible, that is, presence of supplementary motion effects other than breathing. The suggested technique estimates breathing rate with an absolute mean error of 0.03 bmp, regardless of the person's posture. It is clear that the sensing performance improves with the channel diversity, the low-jitter periodic communication, and the oversampling.

13.3.2 Continuous-Wave (CW) Methods

Contrary to packet-based transmissions, continuous-wave (CW) methods radiate a continuous unmodulated EM signal at a specific frequency, thus maximizing the incident power on a target. The energy reflected off the target is detected by another receiving antenna module. The reflected wave is modulated in phase and is used to detect tiny physiological movements induced by breathing and heartbeats.

The early attempts of using CW microwave Doppler radar systems were implemented by Lin in the late 1970s [27, 28]. Lin's first experiment transmits a continuous-wave (CW) signal from 2.1 GHz to 2.5 GHz. The periodic displacement

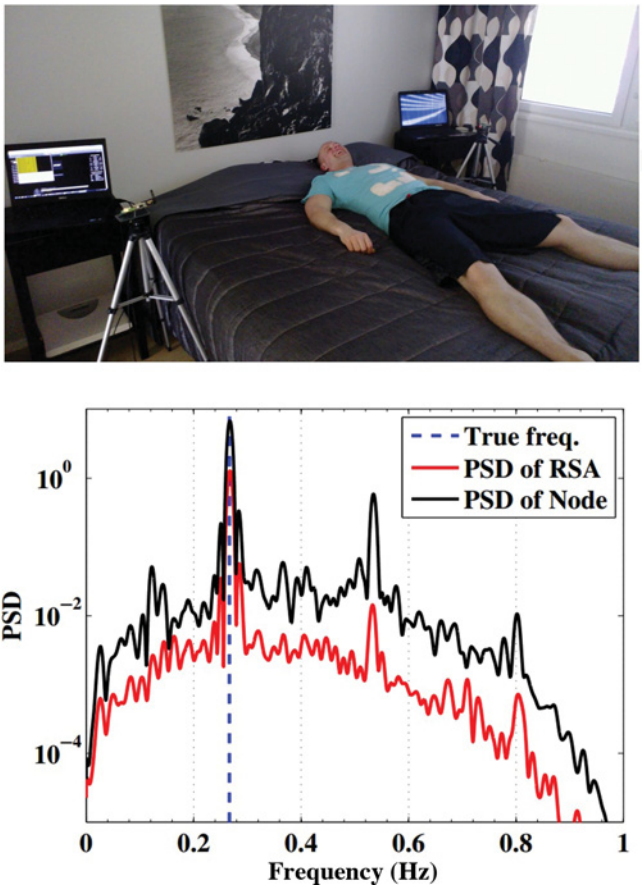

FIGURE 13.10 The experimental setup using one pair of TX-RX nodes and power spectrum density (PSD) of the estimated breathing rate of the test subject. *Source:* Kaltiokallio et al. 2013 [24] and Kaltiokallio et al. 2014 [25]. Reproduced with permission of IEEE.

of the thoracic cavity is recorded in the reflected wave, which is phase modulated (PM) by the time-varying position of the chest (concept related to the Doppler effect, Figure 13.11 [29]).

The phase of the reflected signal off the person's chest is directly proportional to the chest motion and is scaled by the wavelength of the signal. The relation between the chest displacement and the phase variation is modelled by

$$\theta(t) = {}^{4\pi x(t)}/_{\lambda} \tag{13.2}$$

where $\theta(t)$ is the phase of the reflected signal, $x(t)$ is the chest position, and λ is the wavelength of the transmitted EM waves. The information about respiration rate and heart rate is extracted from the recorded phase signal and travelling time.

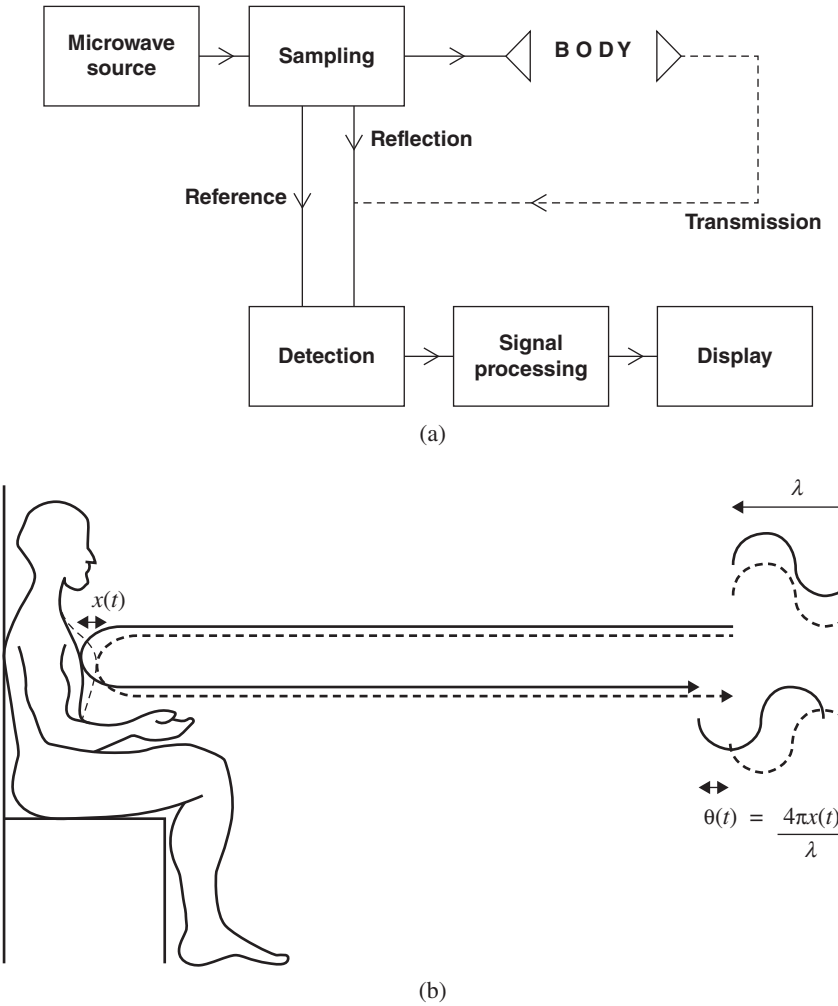

FIGURE 13.11 The principle of CW method: (a) Functional diagrams of a microwave sensing systems for physiological movement and volume change; (b) block diagram of CW radar for non-invasive measurements. *Source:* Lin 1975 [27] and Lin 1979 [28]. Reproduced with permission of IEEE.

Further advances in technology made possible the design of compact and lightweight systems, improving not only the detection accuracy, but also reducing the phase noise of the receiving signal. Doppler radar systems have been tested within academic research environments at 2.4, 5.8, 10, 16, and 60 GHz (Figure 13.12). The proposed system operates up to 1 m from the test subject. Signals are separated using Chebyshev filters and the heart rate variability is estimated by spectral analysis and peak detection methods. The results show that the use of higher frequencies (shorter

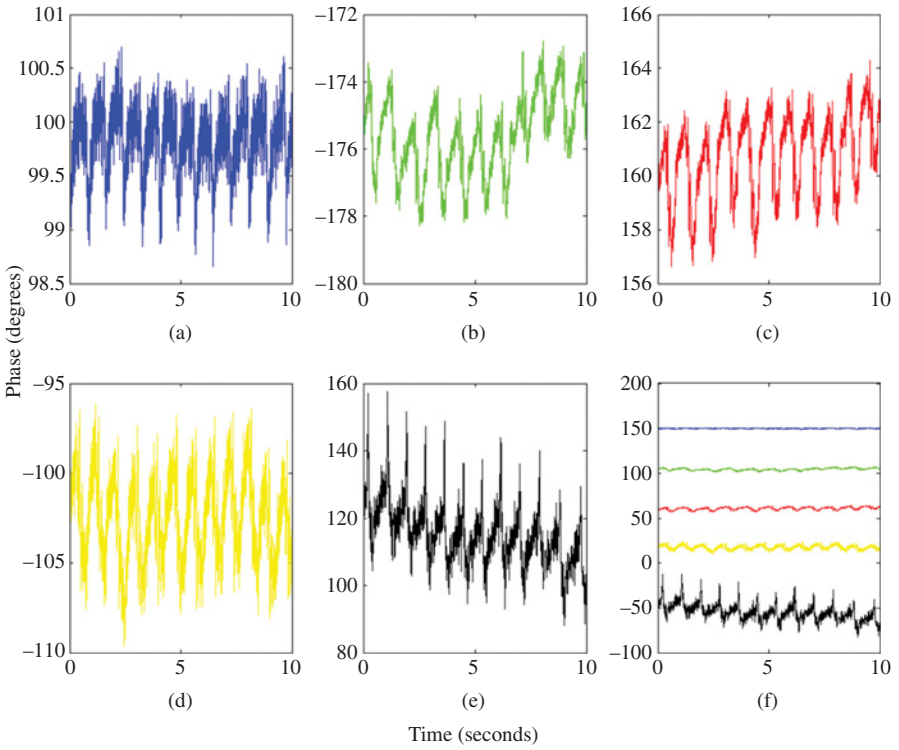

FIGURE 13.12 Contact-less sensing system operating at (a) 2.4 GHz, (b) 5.8 GHz, (c) 10 GHz, (d) 16 GHz, (e) 60 GHz, and (f) heartbeat signal detected from 2.4 GHz up to 60 GHz. *Source:* Obeid et al. 2008 [30] and Obeid et al. 2009 [31]. Reproduced with permission of IEEE.

wavelengths) vastly improve the sensitivity detection levels of the small displacements produced by the chest cavity [30, 31].

Several architectures are experimentally implemented using linear-frequency modulated continuous wave (LFMCW) and frequency-modulated continuous wave (FMCW) which map the differences in time into shifts in the carrier frequency [32, 33]. However, the non-invasive sensing performance of such systems are deterred by nonlinearities of generated frequency ramps as well as the nonlinearities of the voltage-controlled oscillator (VCO).

The combination of such modulation techniques and multiport receiver architectures provide enhanced range resolutions and robustness against clutter and noise. A hybrid six-port radar system operating at 24 GHz CW signal is described in [33]. The radar prototype uses a rectangular horn antenna with a 20 dBi gain (Figure 13.13a). Different measurements are performed with the test subject lying and the six-port radar facing the chest region at a distance of approximately 1 m. The raw results for both physiological signals, breathing, and heartbeat are shown in Figures 13.13b–13.13c. A peak for the respiration rate is evident and the detected

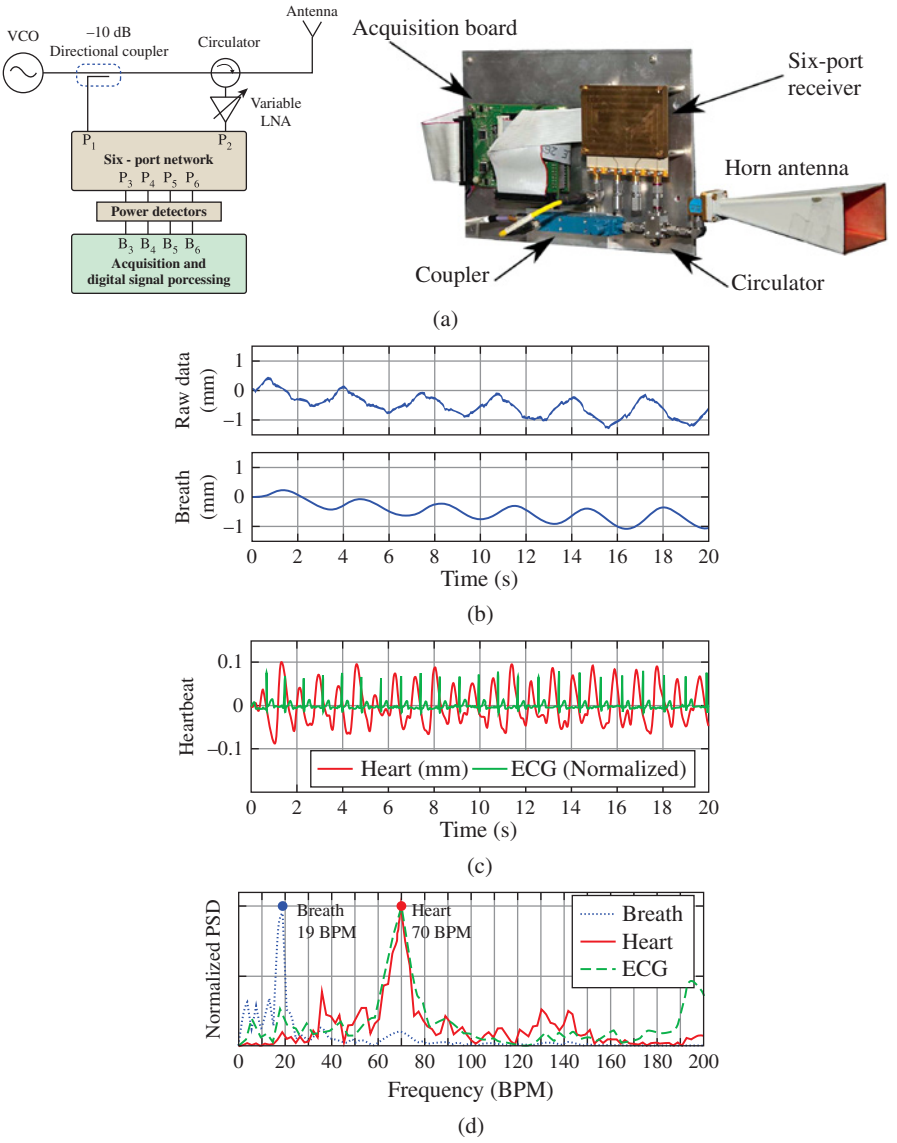

FIGURE 13.13 (a) Schematic of the proposed six-port-based monostatic radar and photograph of the hardware prototype. (b) Time domain signal of the measured raw data and low-pass-filtered breathing signal. The signal delay in the respiration signal is due to the response of the introduced filter; (c) measured heart beat signal in the time domain compared with a reference ECG; (d) Normalized PSD of the measured breath and heart rate signals compared with the PSD of a reference ECG. *Source:* Vinci et al. 2013 [33]. Reproduced with permission of IEEE.

heartbeat rate (70 BPM) is compared with a reference ECG from a medical ECG belt. The plots of normalized PSD for measured breath and heart rate signals are compared with the PSD of a reference ECG (Figure 13.13d).

While the concept of contact-less vital signs detection has been successfully demonstrated, the continuous development and evolution of RF front-end architectures—from heterodyne to homodyne and double-sideband architectures with direct IF sampling and self-injection locking—have enhanced the sensing sensitivity, reduced the interference, and maximized the detection range.

Many prototypes using homodyne double-sideband transmission systems and I/Q modulation (quadrature receivers) show significant reduction on the number of null points associated with single channel Doppler systems [35, 36]. Compact and lightweight CMOS/BiCMOS radar-on-chip solutions operating at 1.6 GHz and 2.4 GHz made use of such quadrature signals (Figure 13.14).

The manufactured chips are capable of detecting the movement produced by the heartbeat and breathing up to 50 cm of distance from the subject. The experimental results also reveal that by using quadrature receivers, the accuracy on heartbeat detection is approximately 80%, a significant improvement over single channel systems.

A high level system integration is shown by Kao's flip-chip CW radar sensor which embeds heterodyne architecture with quadrature demodulation [37]. The micro-radar operates at 60 GHz through a pair of microstrip patch antennas (Figure 13.15). The detection of heartbeat signal has been shown up to 0.3 m from the chest cavity. Although the results are compared to the human counting of the number of beats, complex signal demodulation (CSD) not only eliminates the null detection point problem, but clearly shows the movement of chest cavity due to heartbeat.

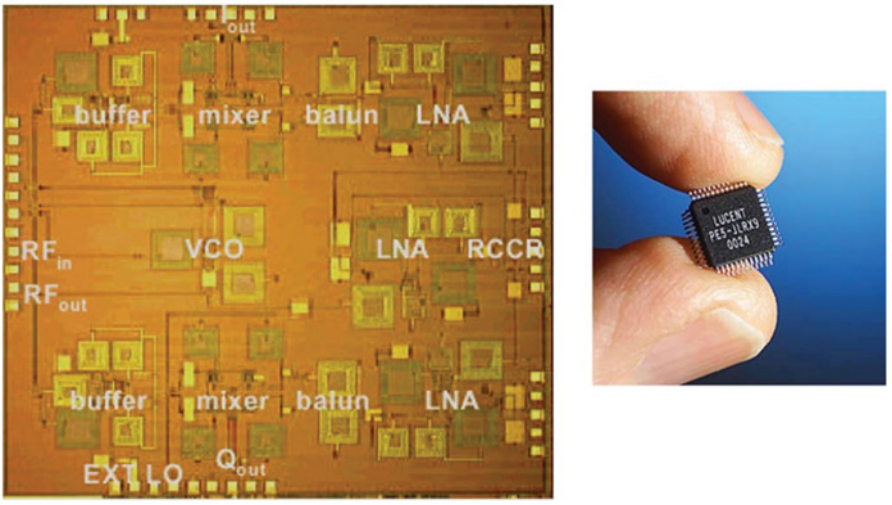

FIGURE 13.14 Photograph of the 0.25 μm silicon CMOS chip operating at 1.6 GHz and 2.4 GHz. *Source:* Droitcour et al. 2004 [34, 35]. Reproduced with permission of IEEE.

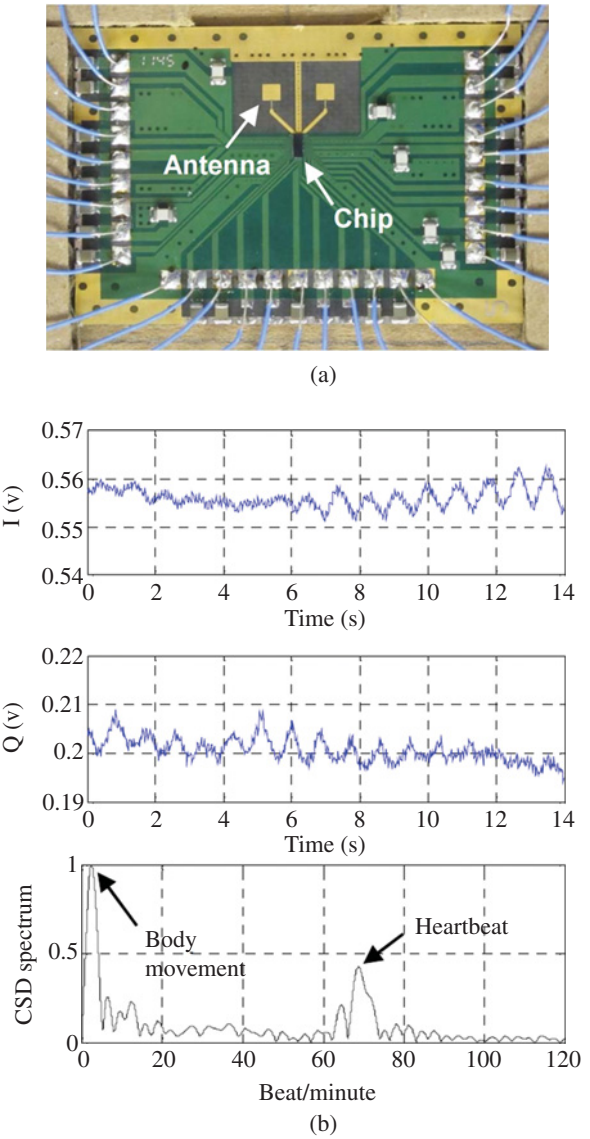

FIGURE 13.15 (a) Photograph of the integrated micro-radar operating at 60 GHz using a heterodyne architecture with quadrature demodulation; (b) baseband IQ outputs of heartbeat signal sampled and displayed by the oscilloscope and CSD spectrum showing heartbeat rate at 69 BPM. *Source:* Kao et al. 2012 [37]. Reproduced with permission of IEEE.

13.3.3 Wide Band Pulsed Radar Method

Ultra-wide band (UWB) pulse-based radio technologies transmit an impulse-like signal over a broad frequency range. When the fractional bandwidth of the transmitted signal is larger than 25% or the absolute bandwidth larger than 500 MHz, the radio signal is considered a UWB [38].

The Federal Communications Commission (FCC) allows the coexistence of UWB systems with existing communication services, such as GPS (global positioning system) and WLAN, but in order to minimize interference with them, UWB technologies must operate at a reduced mean effective isotropic radiated power (EIRP) density level of 41.3 dBm/MHz spread over several GHz of bandwidth [38]. The power spectral density (PSD) of the transmitters need to satisfy specific spectral masks which define the maximum radiated power levels, according to different regulatory bodies around the world (Figure 13.16).

The operation of UWB systems are categorized into two main transmission schemes: single band (impulse radio UWB, IR-UWB) and multiband (multi-carrier UWB). Single-band transmissions can directly modulate short duration pulses with low duty cycles (nanosecond base-band pulses), that can be either pulse amplitude modulation (PAM) or pulse position modulation (PPM), thus reducing the transceiver complexity due to the carrier-less communication.

In contrast to IR-UWB, multiband transmissions divide the UWB frequency band from 3.1 GHz to 10.6 GHz into several small bands, referred as sub-bands, where each sub-band has at least 500 MHz bandwidth (to comply with UWB regulations). The simultaneous transmission of multiple signals is achieved thanks to the digital

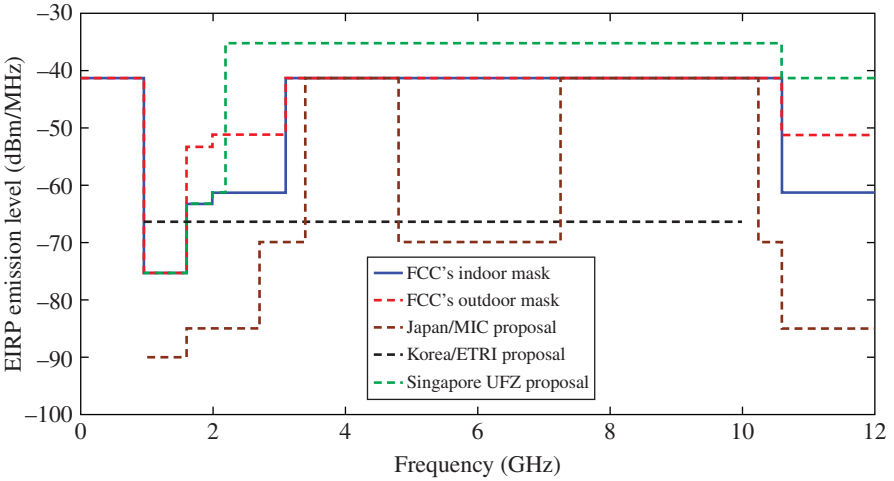

FIGURE 13.16 Proposed spectral masks of different regulatory bodies around the world. *Source:* Federal Communications Commission [38] (Public domain) and Y. Rahayu et al. 2008 [39]. (Reproduced with permission of IEEE).

encoding scheme and the orthogonal frequency division multiplexing (OFDM) (i.e., multi-carrier modulation) [39].

A wide range of UWB applications have been demonstrated and have shown several features that differentiate it from conventional narrowband systems. The high spatial resolution, the reduced inter-symbol interference (ISI), low PSD levels, and immunity to multipath are important characteristics that make UWB systems an alternative solution to CW radars and RSS-based methods for non-invasive physiological sensing.

A UWB transceiver front-end, operating from 3 GHz to 10 GHz, is implemented using standard 130 nm complementary metal oxide semiconductor technology and packaged in a high-frequency cavity. The core area of the transceiver circuit is 500 μm × 1100 μm and integrates a diplexer with a full UWB band carrier-based transmitter, a digital controlled oscillator (for pulse modulation) and a receiver front-end [40] (Figure 13.17a). The respiration patterns are detected from pulses that are

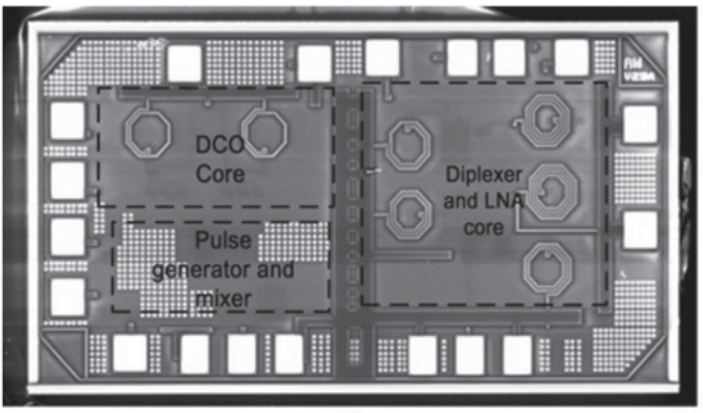

(a)

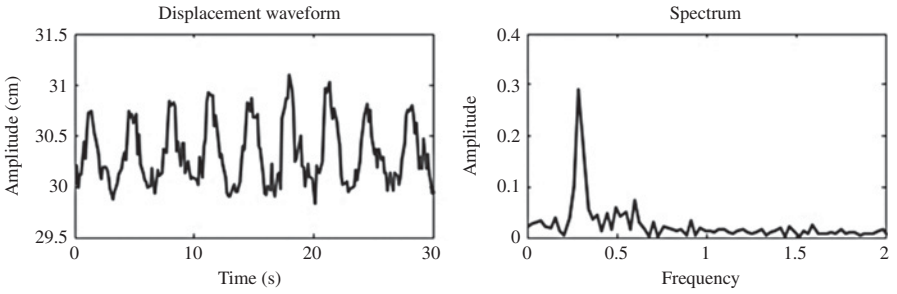

(b)

FIGURE 13.17 (a) Micrograph of the radar transceiver chip; (b) Measured breathing pattern in the time domain and the frequency domain for a time frame of 30 seconds and processed using FFT method. *Source:* Xubo et al. 2014 [40]. Reproduced with permission of IEEE.

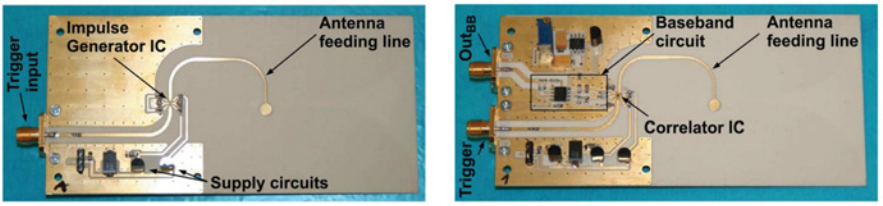

FIGURE 13.18 Photographs of the packaging of the monolithic microwave integrated circuits (MMIC) technology done by chip-on-board mounting on the antenna substrate: (a) compact impulse transmitter with antenna structure on backside; (b) correlation receiver IC and the BB circuit with the receiving the antenna structure on backside. *Source:* Schleicher et al. 2013 [41]. Reproduced with permission of IEEE.

transmitted every 0.1 μs toward the chest of a sitting test subject. The time interval for the transmitted and received signals determines the displacements of the chest movements. Each UWB pulse flight time interval is 4.2 ns which is converted to the distance of movement (Figure 13.19b). The implemented transceiver chip is capable of detecting human breathing within a distance of 50 cm.

Scheleicher et al. implemented an IR-UWB radar using monolithic microwave integrated circuits (MMICs) that are directly connected to 9.3 dBi Vivaldi antennas with an exponentially tapered slot line and a transition to a microstrip line by a Marchand balun. The transmitter structure houses an interpulse generator IC complying with the FCC regulations for indoor masks (Figure 13.18a). The receiver module embeds a correlator IC and a baseband circuit which provide a conversion from differential to single ended as well as the correlation stage (Figure 13.18b) [41]. The advantage of using a hardware correlation principle is that the impulses do not have to be sampled at a picosecond sampling rate, but at a more adequate sampling rate, depending on the frequency difference Δf (small frequency difference applied to the template impulse train in the correlation receiver).

The demonstrator acquires time domain breathing patterns from a male test subject and a 7-week-old infant. The transmitter sensor is mounted on a tripod and the main radiation beam, which emits a train of Gaussian pulses, is pointed toward the test subject's chest from a distance of around 20–25 cm away (Figure 13.19) [41]. For longer distances, the reflected signal decreases slightly in amplitude due to spreading loss, but the sweeping impulse correlation allows a determination of the signals with the same precision.

13.4 DISCUSSION AND CONCLUSION

The chapter summarized potential non-invasive technologies for future smart infrastructures (hospitals, military services, and care centers) supporting EM sensing technologies. The current solutions remain an essential and active part of patient/user awareness, not only to off-load demand of clinical services, but also to promote

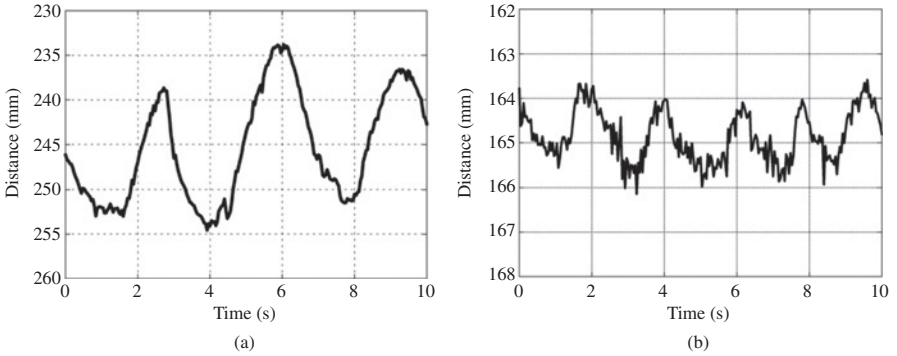

FIGURE 13.19 Time domain experimental results obtained by the IR-UWB radar sensor from (a) male test person breathing normally; (b) 7-week-old sleeping infant showing a sequence with a continuous breathing cycle. *Source:* Schleicher et al. 2013 [41]. Reproduced with permission of IEEE.

autonomous, unobtrusive, and flexible non-invasive monitoring solutions, especially for applications where the monitoring of vital signs are crucial.

Doppler radars adopting packet-based transmissions (RSS values), continuous wave (CW), and pulsed radar (UBW) have been recently introduced to a variety of applications, including home monitoring. Each of these non-invasive radio sensing technologies are described by highlighting the most promising ones. The EM wave travelling from on/off-body radio channels not only contain radio propagation characteristics, but also embed biomechanical information, such as motion pattern, breathing rate, and even heartbeat.

The received power signals, which are a combination of reflected, diffracted, and scattered waves, are highly non-stationary due to the constant change of frequency, amplitude, and phase with traveling time. For example, the continuous movement of the human body, trunk, and the limbs (dynamic scenarios) shadows the line-of-sight propagation, thus producing signal fluctuations of ± 15 dB from the average received signal.

Although received signals present high amplitude variance, different hardware and software methods are described to separate physiological signals. The latter solutions range from the simplest filtering and analysis of spectrum plots (FFT) to the most complex RF front-end architectures, such as homodyne with I/Q baseband modulation. In addition, high level system integration (top-end hardware) are presented from MMIC to CMOS/BiCMOS micro-radar-on-chips.

It is evident that greater sophistication is required in the presence of time-varying clutter and extraneous body movements. The use of powerful and robust digital signal processing techniques (e.g., template matching, blind source separation, and wavelet transforms) is undoubtedly advantageous to reduce the noise, and to extract vital signs successfully (for heart rate) and more accurately (for breathing rate).

There are several challenges that remain to be addressed, aside from making devices more compact. Directive narrow side lobe and higher gain antennas, like

minimizing various noise sources (interference from external clutter), reduce the susceptibility to significant human motion artifacts. They can also achieve higher sensitivity levels with low levels of radiated power and ultimately, the detection of physiological signs on dynamic and outdoor scenarios.

We expect that next generation Doppler radars will integrate hybrid RF front-end architectures using background subtraction spectra algorithms and operating at UWB bands with antennas scanning at multiple frequencies, or even phased array systems, so that the angular coverage is extended up to 180°.

REFERENCES

[1] P. S. Hall and Y. Hao, in *Antennas and Propagation for Body-Centric Wireless Communications*. Artech House, 2006.

[2] Y. Hao and R. Foster, "Wireless body sensor networks for health-monitoring applications," *Physiol. Meas.*, vol. 29, p. R27, 2008.

[3] W. D. Jones, "New biosensor chip picks up heart signals remotely," *IEEE Spectrum, Inst. Electrical and Electron. Engrs.*, vol. 1, 2011.

[4] B. Gyselinckx, C. Van Hoof, J. Ryckaert, R. F. Yazicioglu, P. Fiorini, and V. Leonov, "Human++: Autonomous Wireless Sensors for Body Area Networks," in Proceedings of the IEEE Custom Integrated Circuits Conference, September 18–21, 2005, pp. 13–19.

[5] A. D. Joseph, "Energy harvesting projects," *Pervasive Comput., IEEE*, vol. 4, pp. 69–71, 2005.

[6] L. Xin and Y. Shuang-Hua, "Thermal Energy Harvesting for WSNs," in 2010 IEEE International Conference on Systems Man and Cybernetics (SMC), Istanbul, October 10–13, 2010, pp. 3045–3052.

[7] L. Schwiebert, S. K. S. Gupta, and J. Weinmann, "Research Challenges in Wireless Networks of Biomedical Sensors," in Proceedings of the 7th Annual International Conference on Mobile Computing and Networking, Rome, Italy, 2001.

[8] T. Arampatzis, J. Lygeros, and S. Manesis, "A Survey of Applications of Wireless Sensors and Wireless Sensor Networks," in Proceedings of the 2005 IEEE International Symposium on Intelligent Control, Mediterranean Conference on Control and Automation, Limassol, June 27—29, 2005, pp. 719–724.

[9] A. Pantelopoulos and N. G. Bourbakis, "A Survey on Wearable Sensor-Based Systems for Health Monitoring and Prognosis," *IEEE Transactions on Systems, Man, and Cybernetics, Part C (Applications and Reviews),* vol. 40, pp. 1–12, 2010.

[10] R. S. Hornung, R. F. Mahler, and E. B. Raftery, "Ambulatory blood pressure and heart rate in diabetic patients: an assessment of autonomic function," *Diabet. Med.*, vol. 6, pp. 579–585, October 1989.

[11] H. Forster, O. Ipsiroglu, R. Kerbl, and E. Paditz, "[Sudden infant death and pediatric sleep medicine]," *Wien Klin Wochenschr*, vol. 115, pp. 847–849, December 30 2003.

[12] N. Hafner, I. Mostafanezhad, V. M. Lubecke, O. Boric-Lubecke, and A. Host-Madsen, "Non-Contact Cardiopulmonary Sensing with a Baby Monitor," in 29th Annual International Conference of the IEEE Engineering in Medicine and Biology Society (EMBS), Lyon, August 22–26 2006, pp. 2300–2302.

[13] L. Yee Siong, P. N. Pathirana, and C. L. Steinfort, "Respiration Rate and Breathing Patterns from Doppler Radar Measurements," in 2014 IEEE Conference on Biomedical Engineering and Sciences (IECBES), Kuala Lumpur, December 8–10 2014, pp. 235–240.

[14] C. Kun-Mu, H. Yong, Z. Jianping, and A. Norman, "Microwave life-detection systems for searching human subjects under earthquake rubble or behind barrier," *IEEE Trans. Biomed. Eng.*, vol. 47, pp. 105–114, 2000.

[15] W. L. Kenney, J. Wilmore, and D. Costill, *Physiology of Sport and Exercise,* 6th ed. Human Kinetics Publishers, 2015.

[16] P. J. Maud and C. Foster, *Physiological Assessment of Human Fitness*. Human Kinetics Publishers, 2006.

[17] M. O. Munoz, R. Foster, and H. Yang, "Exploring physiological parameters in dynamic WBAN channels," *IEEE Trans. Antennas Propag.,* vol. 62, pp. 5268–5281, July 2014.

[18] M. Munoz Torrico, R. Foster, and Y. Hao, "Identifying Physiological Features from the Radio Propagation Signal of Low-Power Wireless Sensors," in Wireless Mobile Communication and Healthcare: Third International Conference, MobiHealth 2012, Paris, France, November 21–23, 2012, Revised Selected Papers, B. Godara and K. S. Nikita, Eds., 1 ed Berlin, Heidelberg: Springer Berlin Heidelberg, 2013, pp. 341–350.

[19] P. S. Hall and Y. Hao, *Antennas and Propagation for Body-Centric Wireless Communications*, 2nd ed. Artech House, 2012.

[20] A. R. Guraliuc, P. Barsocchi, X. F. Potorti, and P. Nepa, "Limb movements classification using wearable wireless transceivers," *IEEE Trans. Inf. Technol. Biomed.*, vol. 15, pp. 474–480, February 2011.

[21] A. R. Guraliuc, A. A. Serra, P. Nepa, G. Manara, and F. Potorti, "Detection and Classification of Human Arm Movements for Physical Rehabilitation," in IEEE Antennas and Propagation Society International Symposium (APSURSI), Toronto, July 11–17, 2010, pp. 1–4.

[22] N. Patwari, J. Wilson, S. Ananthanarayanan, S. K. Kasera, and D. R. Westenskow, "Monitoring breathing via signal strength in wireless networks," *IEEE Trans. Mobile Comput.,* vol. 13, pp. 1774–1786, 2014.

[23] N. Patwari, L. Brewer, Q. Tate, O. Kaltiokallio, and M. Bocca, "Breathfinding: a wireless network that monitors and locates breathing in a home," *IEEE J. Sel. Top. Signal Process.,* vol. 8, pp. 30–42, February 2014.

[24] O. Kaltiokallio, H. Yigitler, R. Jäntti, and N. Patwari, "Catch a Breath: Non-invasive Respiration Rate Monitoring via Wireless Communication," *arXiv preprint arXiv:1307.0084,* 2013.

[25] O. Kaltiokallio, H. Yigitler, R. Jantti, and N. Patwari, "Non-invasive Respiration Rate Monitoring Using a Single COTS TX-RX Pair," in IPSN-14 Proceedings of the 13th International Symposium on Information Processing in Sensor Networks, Berlin, April 15–17, 2014, pp. 59–69.

[26] IEEE 802.15.4 Standard. Wireless Medium Access Control (MAC) and Physical Layer (PHY) Specifications for Low Rate Wireless Personal Area Networks (LR-WPANs), 2006. Available at http://standards.ieee.org/getieee802/download/802.15.4-2006.pdf

[27] J. C. Lin, "Noninvasive Microwave Measurement of Respiration," in Proceedings of the IEEE, vol. 63, October 1975, pp. 1530–1530.

[28] J. C. Lin, J. Kiernicki, M. Kiernicki, and P. B. Wollschlaeger, "Microwave apexcardiography," *IEEE Trans. Microw. Theory Techn.*, vol. 27, pp. 618–620, June 1979.

[29] J. C. Lin, "Microwave sensing of physiological movement and volume change: a review," *Bioelectromagnetics*, vol. 13, pp. 557–65, 1992.

[30] D. Obeid, G. Issa, S. Sadek, G. Zaharia, and G. El Zein, "Low Power Microwave Systems for Heartbeat Rate Detection at 2.4, 5.8, 10 and 16 GHz," in First International Symposium on Applied Sciences on Biomedical and Communication Technologies, 2008. ISABEL '08, Aalborg, October 25–28, 2008, pp. 1–5.

[31] D. Obeid, S. Sadek, G. Zaharia, and G. El Zein, "Advances in Microwave Systems for Medical Applications," in International Conference on Advances in Computational Tools for Engineering Applications, 2009. ACTEA '09, Zouk Mosbeh, July 15–17, 2009, pp. 463–468.

[32] W. Guochao, J. M. Munoz-Ferreras, G. Changzhan, L. Changzhi, and R. Gomez-Garcia, "Application of linear-frequency-modulated continuous-wave (LFMCW) radars for tracking of vital signs," *IEEE Trans. Microw. Theory and Tech.,* vol. 62, pp. 1387–1399, 2014.

[33] G. Vinci, S. Lindner, F. Barbon, S. Mann, M. Hofmann, A. Duda, R. Weigel, and A. Koelpin, "Six-port radar sensor for remote respiration rate and heartbeat vital-sign monitoring," *IEEE Trans. Microw. Theory and Tech.,* vol. 61, pp. 2093–2100, 2013.

[34] A. D. Droitcour, O. Boric-Lubecke, V. M. Lubecke, and L. Jenshan, "0.25 /spl mu/m CMOS and BiCMOS Single-Chip Direct-Conversion Doppler Radars for Remote Sensing of Vital Signs," in 2002 IEEE International Solid-State Circuits Conference, ISSCC, San Francisco, CA, February 7–7, 2002, vol. 1, pp. 348–349.

[35] A. D. Droitcour, O. Boric-Lubecke, V. M. Lubecke, J. Lin, and G. T. A. Kovacs, "Range correlation and I/Q performance benefits in single-chip silicon Doppler radars for noncontact cardiopulmonary monitoring," *IEEE Trans. Microw. Theory and Tech.,* vol. 52, pp. 838–848, 2004.

[36] L. Changzhi, X. Yanming, and J. Lin, "Experiment and spectral analysis of a low-power K*a*-band heartbeat detector measuring from four sides of a human body," *IEEE Trans. Microw. Theory and Techn.,* vol. 54, pp. 4464–4471, 2006.

[37] T. Y. J. Kao, A. Y. K. Chen, Y. Yan, S. Tze-Min, and L. Jenshan, "A Flip-Chip-Packaged and Fully Integrated 60 GHz CMOS Micro-Radar Sensor for Heartbeat and Mechanical Vibration Detections," in 2012 IEEE Radio Frequency Integrated Circuits Symposium (RFIC), Montreal, QC, June 17–19, 2012, pp. 443–446.

[38] Federal Communications Commission (FCC) rules and regulations. Title 47: Telecommunication, Part 15: Radio Frequency Devices, Subpart F: Ultra Wideband Operation. (2011). Available at http://hraunfoss.fcc.gov/edocs_public/attachmatch/FCC-02-48A1.pdf

[39] Y. Rahayu, T. A. Rahman, R. Ngah, and P. S. Hall, "Ultra wideband technology and its applications," 2008 5th IFIP International Conference on Wireless and Optical Communications Networks (WOCN '08), Surabaya, 2008, pp. 1–5. doi: 10.1109/WOCN.2008.4542537

[40] W. Xubo, D. Anh, and D. Teng, "3–10 GHz ultra wideband front-end transceiver in 0.13 μm complementary metal oxide semiconductor for low-power biomedical radar," *IET Circuits, Devices & Syst.,* vol. 8, pp. 272–279, 2014.

[41] B. Schleicher, I. Nasr, A. Trasser, and H. Schumacher, "IR-UWB radar demonstrator for ultra-fine movement detection and vital-sign monitoring," *IEEE Trans. Microw. Theory Tech.,* vol. 61, pp. 2076–2085, March 2013.